Holographically Directed Assembly of Polymer Nanocomposites

Abigail T. Juhl,[†] John D. Busbee,[†,‡] John J. Koval,[†] Lalgudi V. Natarajan,[‡] Vincent P. Tondiglia,[‡] Richard A. Vaia,[‡] Timothy J. Bunning,[‡] and Paul V. Braun*,[†]

[†]Department of Materials Science and Engineering, Beckman Institute, Frederick Seitz Materials Research Laboratory, University of Illinois, Illinois 61801, United States, and [‡]Air Force Research Laboratory, Materials and Manufacturing Directorate, Wright-Patterson Air Force Base, Ohio 45433, United States

ARTICLE

ABSTRACT Layered polymer/nanoparticle composites have been created through the one-step two-beam interference lithographic exposure of a dispersion of 25 and 50 nm silica particles within a photopolymerizable mixture at a wavelength of 532 nm. The polymerizable mixture is composed of pentaerythritol triacrylate (monomer), 1-vinyl-2-pyrrolidinone (monomer), and photoinitiator. In the areas of constructive interference, the monomer begins to polymerize *via* a free-radical process and concurrently the nanoparticles move into the regions of destructive interference. The effects of exposure time, power density, nanoparticle size, and periodicity on the final nanocomposite structure were measured with transmission electron microscopy to determine the mechanism for particle segregation. Diffraction from the sample was monitored as well, though its magnitude was not a good predictor of nanostructure in this relatively low index contrast system. Exposure time did not have a strong effect on the final structure. The best nanoparticle sequestration was observed at reduced laser power density, smaller interferogram periodicity, and decreased nanoparticle size, indicating that particle segregation is dominated by diffusion-limited nanoparticle transport directed by a matrix containing a gradient of polymerization kinetics.

KEYWORDS: directed assembly · nanoparticles · nanocomposite · holography · photopolymerization

Nanocomposite materials have been shown to have advanced properties relative to conventional bulk polymeric systems;[1] however, in almost all cases, the nanoscopic elements are randomly distributed; there has only been limited success in fabricating nanocomposites in which the nanoconstituent is arranged in a regular fashion.[2] Explicit control of the arrangement of matter in a nanocomposite material is important for both optical and electrical applications due to the fact that electrical and optical properties are very sensitive to the nanoscale arrangement of matter. It remains a major challenge to efficiently assemble nanosized inorganic species into the complex, hierarchical structures often required for optically and electrically functional materials. Rigorous spatial control of materials in two dimensions can be achieved by many methods including nanoimprint lithography,[3] microcontact printing,[4] and e-beam writing,[5] but extending this to three dimensions usually involves time-consuming multistep processing. Other techniques which can add structure to a nanocomposite system, including shear,[6] and external electric[7] or magnetic[8] fields require either inorganic moieties that lack translational symmetry or the use of a structured matrix, such as a block copolymer.[9] However, there is now promising evidence that a one-step holographic method can be used to spatially control the position of nanoparticles within a three-dimensional polymer nanocomposite.

Several years ago, Vaia et al. demonstrated the formation of polymer nanocomposites containing periodic layers of 5 nm gold nanoparticles, 260 nm polystyrene spheres, and clays.[10] Other groups have assembled zirconia,[11−13] titania,[12,14,15] doped $LaPO_4$,[16] silica,[17,18] semiconductor,[19] and zeolite[20,21] nanoparticles *via* holography. In all cases, nanoparticles are added into a mixture of monomer, photoinitiator, and co-initiator. Upon holographic illumination, the photoinitiator in the regions of high intensity forms radicals which initiate polymerization. Polymerization decreases the concentration of the monomers in the high intensity regions causing a net flux of monomers into that region. As the monomers react, the unreactive, mobile species move into the regions of low intensity (Figure 1). This movement of the monomers toward regions of constructive interference and nanoparticles toward regions of destructive interference was shown experimentally by Tomita and Suzuki.[22,23]

Tomita and Suzuki's phase shift measurement[22,23] shows clearly that the nanoparticles move into the low-intensity

*Address correspondence to pbraun@illinois.edu.

Received for review April 26, 2010 and accepted September 27, 2010.

Published online October 7, 2010.
10.1021/nn100885x

© 2010 American Chemical Society

Report Documentation Page

Form Approved
OMB No. 0704-0188

Public reporting burden for the collection of information is estimated to average 1 hour per response, including the time for reviewing instructions, searching existing data sources, gathering and maintaining the data needed, and completing and reviewing the collection of information. Send comments regarding this burden estimate or any other aspect of this collection of information, including suggestions for reducing this burden, to Washington Headquarters Services, Directorate for Information Operations and Reports, 1215 Jefferson Davis Highway, Suite 1204, Arlington VA 22202-4302. Respondents should be aware that notwithstanding any other provision of law, no person shall be subject to a penalty for failing to comply with a collection of information if it does not display a currently valid OMB control number.

1. REPORT DATE **07 OCT 2010**	2. REPORT TYPE	3. DATES COVERED **00-00-2010 to 00-00-2010**
4. TITLE AND SUBTITLE **Holographically Directed Assembly of Polymer Nanocomposites**		5a. CONTRACT NUMBER
		5b. GRANT NUMBER
		5c. PROGRAM ELEMENT NUMBER
6. AUTHOR(S)		5d. PROJECT NUMBER
		5e. TASK NUMBER
		5f. WORK UNIT NUMBER
7. PERFORMING ORGANIZATION NAME(S) AND ADDRESS(ES) **University of Illinois at Urbana-Champaign,Beckman Institute,Department of Materials Science and Engineering,Urbana,IL,61801**		8. PERFORMING ORGANIZATION REPORT NUMBER
9. SPONSORING/MONITORING AGENCY NAME(S) AND ADDRESS(ES)		10. SPONSOR/MONITOR'S ACRONYM(S)
		11. SPONSOR/MONITOR'S REPORT NUMBER(S)

12. DISTRIBUTION/AVAILABILITY STATEMENT
Approved for public release; distribution unlimited

13. SUPPLEMENTARY NOTES

14. ABSTRACT

Layered polymer/nanoparticle composites have been created through the one-step two-beam interference lithographic exposure of a dispersion of 25 and 50 nm silica particles within a photopolymerizable mixture at a wavelength of 532 nm. The polymerizable mixture is composed of pentaerythritol triacrylate (monomer), 1-vinyl-2-pyrrolidinone (monomer), and photoinitiator. In the areas of constructive interference, the monomer begins to polymerize via a free-radical process and concurrently the nanoparticles move into the regions of destructive interference. The effects of exposure time, power density, nanoparticle size, and periodicity on the final nanocomposite structure were measured with transmission electron microscopy to determine the mechanism for particle segregation. Diffraction from the sample was monitored as well, though its magnitude was not a good predictor of nanostructure in this relatively low index contrast system. Exposure time did not have a strong effect on the final structure. The best nanoparticle sequestration was observed at reduced laser power density smaller interferogram periodicity, and decreased nanoparticle size, indicating that particle segregation is dominated by diffusion-limited nanoparticle transport directed by a matrix containing a gradient of polymerization kinetics.

15. SUBJECT TERMS

16. SECURITY CLASSIFICATION OF:			17. LIMITATION OF ABSTRACT	18. NUMBER OF PAGES	19a. NAME OF RESPONSIBLE PERSON
a. REPORT **unclassified**	b. ABSTRACT **unclassified**	c. THIS PAGE **unclassified**	**Same as Report (SAR)**	**9**	

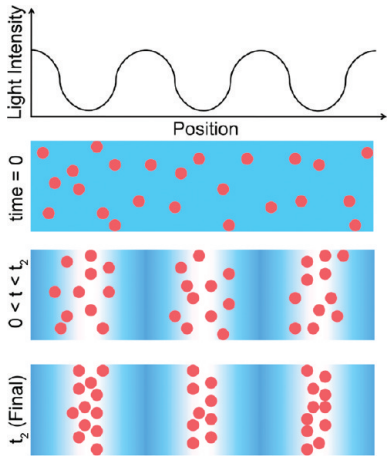

Figure 1. Spatial distribution of nanoparticles as a function of time when exposed to a periodically varying light intensity distribution. Before laser exposure at time (t) = 0, nanoparticles are homogeneously distributed throughout the sample. Polymerization is then induced by the optical interference pattern. The constructive interference regions of the sample polymerize first, leading to sequestration of monomer toward the high intensity regions and nanoparticles toward the low intensity regions ($0 < t < t2$). Photopolymerization eventually occurs even in the low intensity regions, locking the nanoparticles in place ($t2$ = final).

regions and monomer moves into the regions of high intensity. The mechanism for nanoparticle movement, however, is unclear. Possible reasons for nanoparticle transport include nanoparticle phase separation as monomer is polymerized, monomer transport into the polymerizing regions leading to sequestration of the nanoparticles into the low intensity regions (conservation of volume), and diffusion-limited mass transport in a matrix containing a gradient of polymerization kinetics. To determine the dominant mechanism, it is necessary to quantitatively determine the final nanoparticle positions as a function of exposure geometry, exposure time, exposure power density, grating periodicity, particle size, and nanoparticle concentration. Although a number of materials systems have been demonstrated *via* this method, the majority of the reports to date have only used diffraction efficiency to estimate the positions of nanoparticles within the photopolymer. However, Goldenberg et al. showed that the diffraction efficiency was not always a good predictor of nanoparticle sequestration.[24] In only a few systems have measurements of the spatially varying nanoparticle concentration been obtained,[16,20,25,26] and only rarely have real-space images been obtained with sufficient resolution to show individual nanoparticles.[10,24] In the work reported here, diffraction measurements are compared with corresponding transmission electron microscopy (TEM) micrographs to determine if the magnitude of the diffraction spots is a good predictor of nanostructure. We find that the magnitude of diffraction is altered by factors other than nanoparticle assembly, and thus only TEM was used to characterize nanoparticle assembly. We demonstrate the effect of exposure geometry, time,

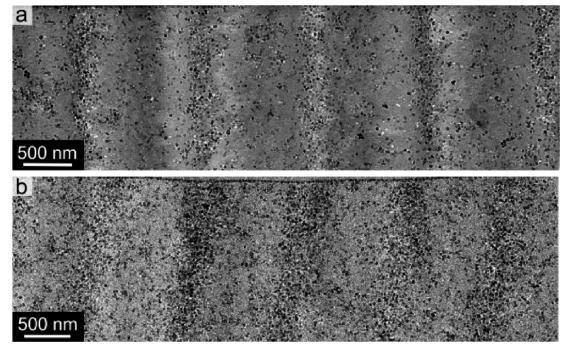

Figure 2. TEM micrographs of holographically photopolymerized samples containing (a) 12.8 wt % and (b) 22.7 wt % 25 nm SiO_2, using a 300 s 2-beam exposure at 200 mW/cm^2 per beam.

power density, periodicity, particle size, and nanoparticle concentration on final nanoparticle positions within the photopolymer, and from this determine the primary mechanism for nanoparticle sequestration is neither nanoparticle phase separation due to conversion of monomer to polymer, nor conservation of volume as monomer diffuses into the polymerizing regions of the sample. The best nanoparticle sequestration occurred using low exposure power densities, short periodicities, and the smaller nanoparticles. Exposure time and nanoparticle concentration did not have a large effect on the final nanoparticle assembly. These results indicate that nanoparticle segregation is a diffusion-limited nanoparticle transport process, most likely driven by gradients in polymerization kinetics under holographic illumination, and guided by Stokes−Einstein dynamics.

RESULTS AND DISCUSSION

A study of the fundamental mechanism for the holographic nanoparticle assembly required development of a silica nanoparticle containing system that would not aggregate under the various experimental conditions. Previous systems incorporating mixtures of multifunctional and monofunctional acrylates such as SR399 and isooctylacrylate were considered,[16] but the unfunctionalized 25 nm silica nanoparticles aggregated in these systems. The other system developed by Tomita was not commercially available and therefore not considered.[25] A new experimentally simple system was developed containing the monomers pentaerythritol triacrylate (PETA) and 1-vinyl-2-pyrrolidinone (NVP), silica nanoparticles, and photoinitiator. The bare silica nanoparticles disperse within the PET/NVP mixture. Figure 2a is a TEM micrograph of a sample consisting of 12.8 wt % 25 nm diameter silica particles, 44.9 wt % PETA, 38.5 wt % NVP, and 3.8 wt % photoinitiator that was polymerized by using two-beam interference from a 532 nm laser. The nanoparticle concentration has been increased to 22.7 w% silica in Figure 2b. Each sample was exposed for 300 s with each beam having a power density of 200 mW/cm^2. High- and low-density

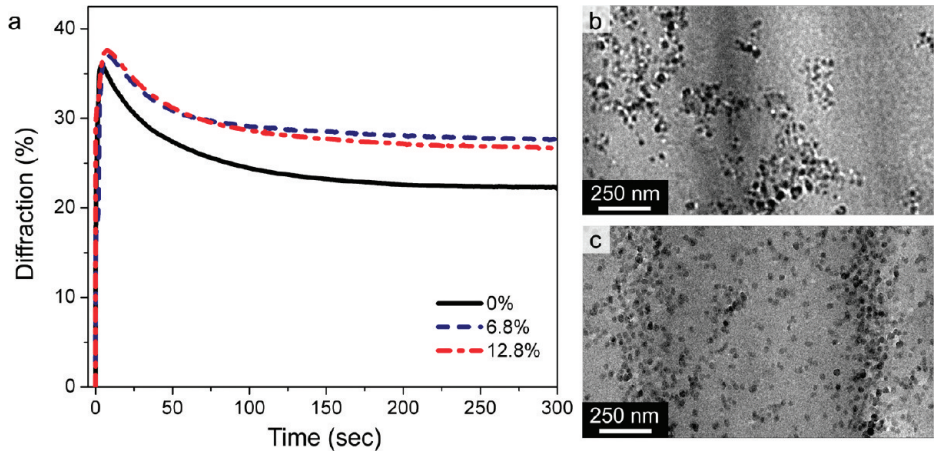

Figure 3. (a) Diffraction intensity of the first-order diffraction peak divided by the sum of the zero- and first-order peaks as a function of exposure time for different concentrations of nanoparticles. (b, c) Corresponding TEM micrographs of samples containing 6.8 and 12.8 wt % 25 nm SiO_2 nanoparticles, respectively. The 12.8 wt % sample shows nanoparticle assembly while the 6.8 wt % sample only shows agglomerations.

silica nanoparticle layers are apparent, and the pitch of the layers was slightly larger than 1 μm, matching the pitch of the interferogram.

Diffraction Measurements. Diffraction measures the index contrast between periodic alternating layers of material. The silica particles have an index of refraction (n) of ~1.46, which is similar to that of the monomers, $n \approx 1.5$. With this low of an index contrast, a high intensity diffracted beam is not expected, but it is still interesting to consider if the magnitude of the diffracted beam can be used to characterize the degree of nanoparticle assembly. To determine if diffraction is a good predictor of nanoparticle assembly, the magnitude of the diffraction from the +1 order and 0 order was monitored while writing the hologram into samples containing various nanoparticle concentrations, and correlated to the TEM determined nanoparticle distribution. Diffraction curves of samples containing different nanoparticle concentrations can be seen in Figure 3a. Over the first few seconds there is a rapid increase in the diffraction magnitude followed by a steady decrease, which has been attributed to slow polymerization of monomers in the darker regions of the sample.[27] We did not always see a decrease in the diffraction curve; this was the case for example when exposures were done at low power densities or with high nanoparticle concentrations (>20 wt %). Most germane to the discussion here, however, is that the magnitude of the diffraction was virtually the same for samples containing either 6.8 wt % agglomerated nanoparticles or 12.8 wt % nonagglomerated nanoparticles. The agglomerated nanoparticles do not assemble into regions of destructive interference, while the 12.8 wt % assemble as expected (Figure 3b,c). If diffraction magnitude was a strong function of nanoparticle assembly, the diffraction curves of these two samples should be significantly different. This was not the case. The diffraction magnitude in both samples is probably caused by monomer segregation due to differences in their polymerization rates. Goldenberg et al. showed that higher fractions of monofunctional acrylate monomer are sequestered into the regions of destructive interference just as the nanoparticles are,[24] and this is probably the origin of the diffraction magnitude in our samples. To evaluate the maximum contribution of the nanoparticles to the diffraction curve, the diffraction magnitude as a function of time was recorded for a nanoparticle free sample (Figure 3a). At most, a 10% change in diffraction magnitude can be attributed to the addition of nanoparticles. The 10% diffraction magnitude change may not even be completely due to nanoparticle assembly, as it has also been shown that the nanoparticles can promote polymer segregation as well.[24] Therefore, diffraction will not be used to characterize the assembly of nanoparticles since other non-nanoparticle effects can alter the absolute magnitude of the measurement. The shape of the diffraction curve can be used to investigate the kinetics of the photopolymerization, but the final positions of the nanoparticles should be determined by using a different approach, for example TEM.

Polymer/Nanoparticle Miscibility Mechanism. With a stable nanoparticle containing photopolymerizable system, coupled with TEM characterization, it was possible to study the fundamental mechanism for nanoparticle sequestration. One possible driving force for nanoparticle assembly is a decrease in the "miscibility" of the nanoparticles as monomer is converted to polymer. If this mechanism dominates, then a flood lit exposure is expected to show large particle aggregations. Figure 4 is a TEM image of a flood lit exposure of a sample containing 12.8 wt % 25 nm diameter silica particles, 44.9 wt % PETA, 38.5 wt % NVP, and 3.8 wt % photoinitiator that was polymerized for 300 s with one beam from a 532 nm laser with a power density of 400 mW/cm^2. These exposure conditions were chosen to match the average power density of the sample shown in Figure 2a, so

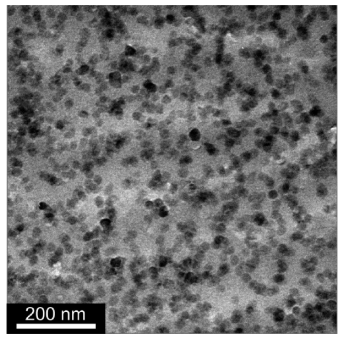

Figure 4. TEM image of a flood lit exposure of a sample containing 12.8 wt % 25 nm diameter silica particles, 44.9 wt % PETA, 38.5 wt % NVP, and 3.8 wt % photoinitiator that was polymerized for 300 s, using one beam from a 532 nm laser with a power density of 400 mW/cm^2.

single-beam and interferometric exposures could be directly compared. There may be minor agglomerations in the silica nanoparticles of the flood-lit sample, but the density of the aggregations is not sufficient to account for the nanoparticle assembly indicating nanoparticle immiscibility is not the dominant mechanism for nanoparticle sequestration.

Although we do not attribute the primary mechanism to liquid-gel demixing, the frontal nature of the polymerization process may cause a similar type of phase separation. If a liquid-gel front moves through the sample it could essentially "sieve" the nanoparticles into the regions of low-intensity light. A flood exposure creates a uniform gelation without a liquid-gel front, so this mechanism would not result in regions of high-density particles. However, for the sinusoidal interferogram we impose on the sample, we expect the result of this mechanism to be more binary, that is, we would expect significant aggregations of nanoparticles in low-intensity light regions and almost no particles in high-intensity regions, rather than the smooth gradient in the nanoparticle density across the period seen in Figure 2. We would also expect this mechanism to work at long length scales, which does not occur as we show later.

Monomer Transport Mechanism. Another possible mechanism for nanoparticle assembly is that nanoparticles are effectively pushed into the regions of destructive interference to conserve volume as the monomers diffuse toward the regions of high-intensity light and polymerize. To test this hypothesis, the assembly of 25 and 50 nm particles was compared. If monomer transport dominates nanoparticle assembly, and thus particle size and particle mobility are no longer important, then 25 and 50 nm particles should assemble under similar photopolymerization conditions. At an exposure power density of 400 mW/cm^2, the 25 nm silica particles sequestered into the regions of destructive interference, but the 50 nm particles did not show any structuring (Figure 5). To assemble the larger particles, the power density had to be reduced to 0.07 mW/cm^2. This suggests nanoparticle assembly is a function of particle mobility, rather than monomer transport. If monomer transport to the polymerizing regions is not the driving force for nanoparticle assembly, then nanoparticle assembly can only occur while the viscosity of the matrix is low enough to allow particle motion. In our system, a three-dimensional network of branched polymer chains forms, leading to a point in which the matrix gels and diffusion can no longer occur. This gel point probably occurs within the first few seconds of exposure at 400 mW/cm^2. Since the 50 nm particles move more slowly than the 25 nm particles, a longer time was needed for nanoparticle sequestration before matrix gelation. Decreasing the power density slowed the polymerization kinetics enough to allow the larger particles to assemble. Due to light scattering by the 50 nm particles, nanoparticle assembly only occurred near the surface of the sample; however, this is only a practical problem and not something that impacted our analysis. In comparing the TEM images of the 25 and 50 nm samples in Figure 5a,b, there is an obvious change in the appearance between the high- and low-intensity regions sample. We suspect that the microtoming of the sample containing larger particles into 90 nm thick sections left holes within the destructive re-

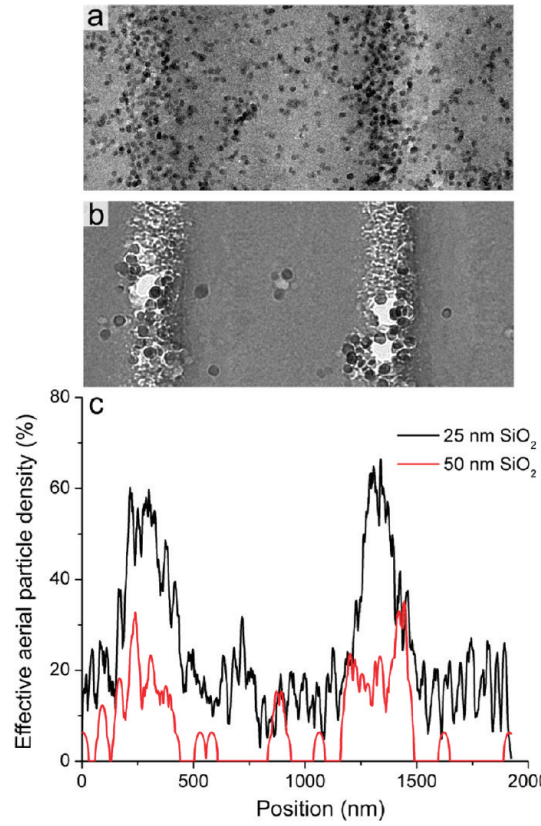

Figure 5. (a, b) TEM micrographs of samples containing 12.8 wt % SiO_2 photopolymerized for 300 s: (a) 25 nm SiO_2 at an exposure power density of 400 mW/cm^2 and (b) 50 nm SiO_2 at an exposure power density of 0.07 mW/cm^2. (c) Graph of the effective aerial nanoparticle density as a function of position extracted from parts a and b. The *x*-axis in panel c is to scale with both TEM micrographs.

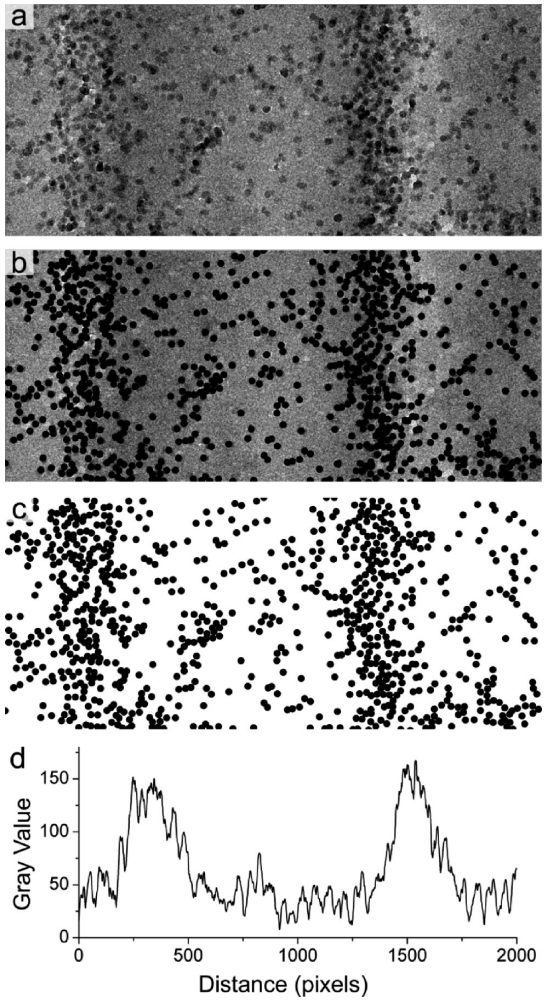

Figure 6. Example of the process used to determine aerial nanoparticle density. (a) Original TEM micrographs were imported into Adobe Photoshop and cropped to 1923 nm by 828 nm. (b) Black circles corresponding to the nanoparticle diameter (25 or 50 nm) placed onto each nanoparticle. (c) The background was then deleted and the dots were placed on a white background. (d) The images with black dots on a white background were then imported into ImageJ and the colors were inverted. The images were then analyzed by using "plot profile", and the gray value was graphed versus distance (in pixels). The gray value was then divided by the total number of pixels to get aerial nanoparticle density, and the pixel number was then correlated to the actual length of the TEM micrograph.

gions of the sample. The positions of the nanoparticles were measured from the TEM micrographs and plotted in Figure 5c. A quantitative understanding of the nanoparticle segregation was obtained through image analysis on each of the TEM micrographs as outlined in Figure 6. Each nanoparticle on the micrograph was treated as a 25 or 50 nm circle, and the effective aerial particle density was measured using ImageJ and plotted against position (Figure 5c). The samples were 90 nm thick so nanoparticles can overlap in the TEM micrograph. Overlapping particles were not counted, so the number of nanoparticles, primarily in the high-intensity regions, is artificially low. To demonstrate that the TEM micrograph in Figure 5a is representative, 5 TEM micrographs from different positions on sample a in Figure 5 are added in the Supporting Information (Figure S1).

Diffusion-Limited Mass Transport Mechanism. On the basis of the experiments with different size nanoparticles and the lack of aggregation under flood exposure, we suggest nanoparticle sequestration is primarily based on nanoparticle transport in a matrix containing a spatially varying gradient of polymerization kinetics. As the matrix polymerizes and gels in the high-field region, movement of nanoparticles toward that region should be greatly suppressed, while transport away from that region should remain allowed. To confirm this hypothesis, the exposure time, power density, and periodicities were varied to study the effects on the final nanoparticle assembly. Exposure times ranged from 6.75 to 300 s, the exposure power densities ranged from 1.6 to 300 mW/cm^2, and the interferogram spacings were 0.5, 1, and 2 μm.

Assuming diffusion-limited mass transport is the primary mechanism for nanoparticle assembly, exposure time should only effect nanoparticle sequestration if the laser interferogram is turned off before gelation has locked the nanoparticles in place. The effect of exposure time on the final nanoparticle positions was studied *via* TEM to obtain a qualitative understanding of the temporal evolution of the nanoparticle positions. Figure 7a is a TEM micrograph of a sample exposed holographically for 6.75 s. Despite the short exposure time, there are still definite high-density regions of 25 nm silica particles periodically spaced about a micrometer apart, and the overall structure is similar to a sample exposed for 300 s (Figure 7b). The spatial distribution of nanoparticles in both images is nearly identical (Figure 7c). The aerial particle density for Figure 7b was determined for 5 separate TEM micrographs of the same sample for a total of 10 regions of high nanoparticle density. The aerial particle density peaks at ~67.4% with a standard deviation of 5.75% in regions of low intensity, and 15−20% in the regions of high intensity. Most of the nanoparticle sequestration must occur in the first 6.75 s, and further increases in exposure time, despite the fact that some of the monomer has not polymerized at 6.75 s, do not have an effect on the final nanoparticle positions, supporting the hypothesis that the nanoparticle movement is driven by particle transport away from the polymerization front, and not monomer diffusing into the polymerizing region.

If nanoparticle transport away from the polymerizing regions is limited by biased Brownian motion,[28] lowering the exposure power density should slow the polymerization rate and increase the time before gelation. Therefore, samples exposed at lower power densities should have better nanoparticle sequestration. The effect of exposure power density was investigated by using interferograms with a total power density of 1.6 and 400 mW/cm^2, Figure 7, parts d and e, respectively.

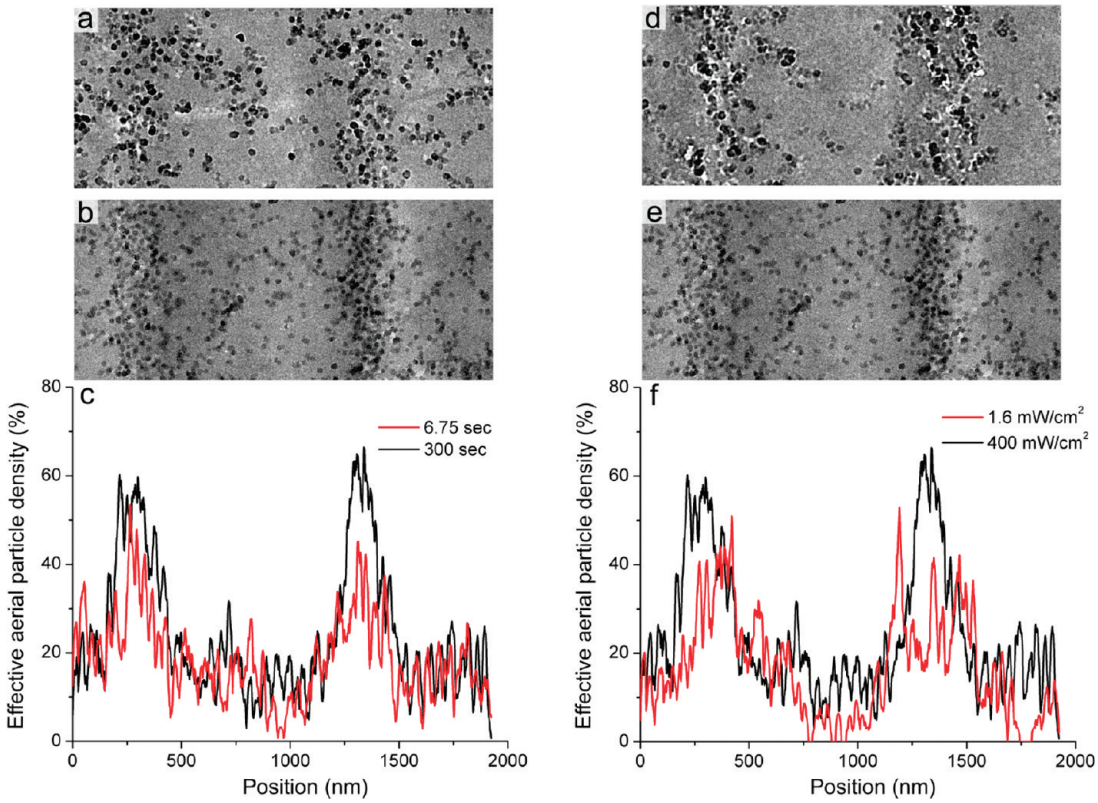

Figure 7. (a, b) TEM micrographs of samples containing 12.8 wt % 25 nm SiO_2 photopolymerized at 400 mW/cm^2 (~1 μm periodicity) for (a) 6.75 and (b) 300 s. (c) Graph of the effective aerial nanoparticle density as a function of position extracted from parts a and b. The *x*-axis in panel c is to scale with both TEM micrographs. (d, e) TEM micrographs of samples containing 12.8 wt % 25 nm SiO_2 photopolymerized for 300 s (~1 μm periodicity) at an exposure power density of (d) 1.6 and (e) 400 mW/cm^2. (f) Graph of the effective aerial nanoparticle density as a function of position extracted from panels d and e. The *x*-axis in panel f is to scale with both TEM micrographs.

As expected, both power densities provided alternating layers of high- and low-density SiO_2. The nanoparticle effective aerial particle density was measured as a function of position (Figure 7f). The lower power density exposure generated a greater degree of nanoparticle sequestration as shown by the fact that there were fewer nanoparticles in the high-intensity regions. The effective aerial density of the low power density sample nearly reaches zero density in the high-intensity regions, while in the high power density sample it remains above 10%. Very few nanoparticles remained in the high-intensity regions of the lower exposure power density sample, presumably because they had time to segregate into the low-intensity regions before they were trapped by gelation of the matrix.

If we assume that transport of nanoparticles is diffusion-limited, then lowering the exposure power density should slow the reaction rate and give more time for nanoparticle sequestration. As just demonstrated, when an exposure power density of 1.6 mW/cm^2 was coupled with a long exposure time (300 s), nanoparticle assembly occurred. But if the lower exposure power density was coupled with a short exposure time, would the samples still sequester? A sample with 12.8 wt % 25 nm SiO_2 was photopolymerized at 1.6 mW/cm^2 for 6.75 s with a 1 μm periodicity (Figure 8). The effective aerial particle density was determined and plotted versus position. Although the sequestration was not as strong as for the sample exposed for 300 s, it is clear that nanoparticle assembly occurs rapidly even under low exposure power densities.

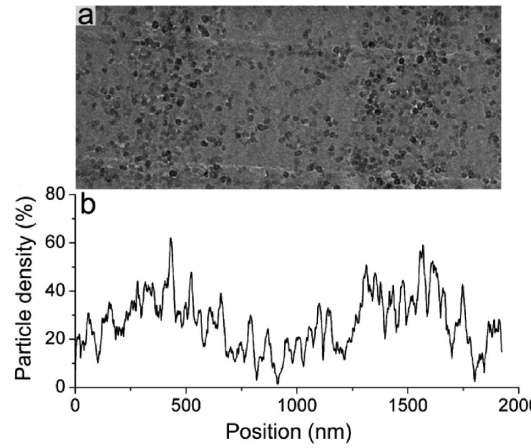

Figure 8. (a) TEM micrograph of a sample containing 12.8 wt % 25 nm SiO_2 photopolymerized at 1.6 mW/cm^2 (~1 μm periodicity) for 6.75 s. (b) Graph of the effective aerial nanoparticle density as a function of position extracted from panel a.

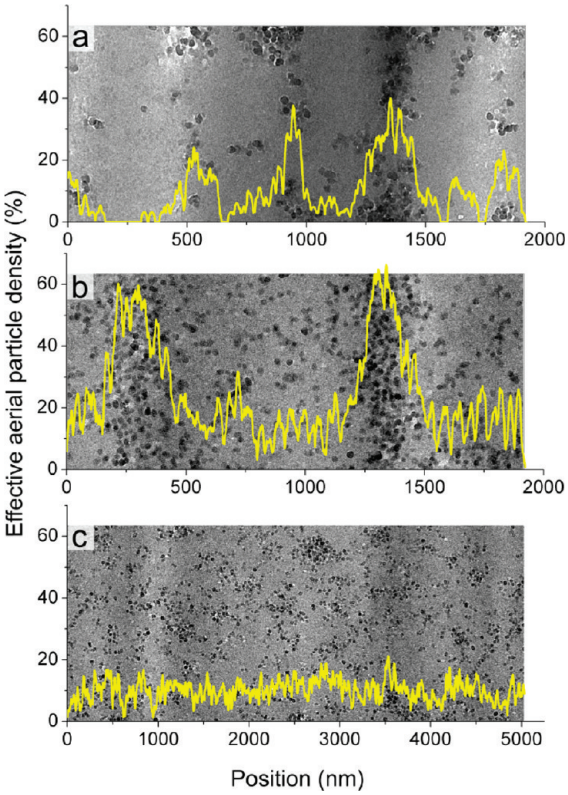

Figure 9. TEM micrographs of samples containing 12.8 wt % 25 nm SiO_2 photopolymerized for 300 s at an exposure power density of 400 mW/cm^2 at periodicities of (a) 500, (b) 1000, and (c) 2000 nm. The effective aerial nanoparticle density as a function of position is plotted over each micrograph. The *x*-axis is to scale for each TEM micrograph.

Finally, if the nanoparticles must move through the polymerizing matrix into the regions of low intensity, then there should be a maximum hologram periodicity after which the nanoparticles could not move the distance necessary before gelation locks them in place. Smaller periodicities should show better sequestration since the particles have the same time to diffuse a shorter distance. To test this assumption, the periodicity was reduced from about 1 μm to 500 nm by increasing the angles of incidence of the interfering beams. Figure 9a is a TEM micrograph of the sample with 500 nm periodicity. Relative to samples with 1 μm periodicity exposed using similar conditions (Figure 9b) there are very few nanoparticles within the constructive interference regions of the 500 nm sample. The nanoparticles in the 500 nm periodic sample had the same amount of time to move before gelation as did the 1 um periodic sample, but the silica did not have to move as far to reach the low-intensity regions. More of the nanoparticles in the sample with small periodicity were displaced to their appropriate positions before gelation locked them in place. As the periodicity was increased to 2 μm (Figure 9c), the nanoparticles did not diffuse into the low-intensity regions and the nanoparticle density does not seem to fluctuate with position. As expected, best nanoparticle sequestration occurs at smaller periodicities.

Stokes−Einstein Predictions. To help understand the limits of nanoparticle transport within our system, Stokes−Einstein dynamics were compared to experimental observations. The viscosity of the nanoparticle/monomer resin before polymerization was measured at 0.07 Pa · s, using a parallel plate rheometer. Assuming that nanoparticle transport is governed by Stokes−Einstein diffusion, the diffusion constant of the nanoparticles in the photocurable resin can be estimated at 0.25 μm^2/s. The Stokes−Einstein diffusion constant was determined by:

$$D = \frac{k_B T}{6\pi\eta r} \quad (1)$$

where k_B is Boltzmann's constant, T is temperature (295 K), η is viscosity, and r is the radius of the nanoparticle (12.5 nm). To estimate the distance that the nanoparticles can diffuse before gelation, the following equation was used:

$$\text{distance diffused} = \sqrt{Dt} \quad (2)$$

t is a measure of time before gelation, which was assumed to be 1−4 s, giving an estimated diffusion distance of 0.5−1 μm. This is most likely greater than the actual value because it does not account for the increase in viscosity before gelation, which increases exponentially with time.[29,30] The maximum diffusion distance observed was approximately 0.5 μm (Figure 9c), which is in reasonable agreement with the Stokes−Einstein predictions.

CONCLUSIONS

The holographically defined assembly of nanoparticle−polymer composites was studied using a new nanocomposite system. In this system, the magnitude of the diffraction was not a good indicator of the actual structure, so TEM imaging was used to evaluate the degree of nanoparticle assembly. The mechanism for nanoparticle movement was studied by changing exposure geometry, exposure time, exposure power density, nanoparticle size, and periodicity. The primary mechanism for nanoparticle assembly was determined to be diffusion-limited nanoparticle transport in an optically defined gradient of polymer density. This is supported by the fact that exposure time did not affect the resulting structure, while lowering exposure power density, decreasing nanoparticle size, and smaller interferogram periodicity all gave better nanoparticle sequestration. Stokes−Einstein dynamics were a good guide for determining maximum nanoparticle diffusion distances. Although the low-contrast system may not be pertinent to applications which require high diffraction efficiencies, it does explicitly highlight the relationship between the kinetics of the polymerization

and the structures formed in polymerization-induced nanoparticle assembly.

METHODS

The 25 nm silica particles were prepared by mixing 240 mL of ethanol (Decon Laboratories INC, cat. no. 2701), 3 mL of deionized water, and 6 mL of ammonium hydroxide (Aldrich, cat. no. 329145). Under rapid stirring, 6 mL of tetraethyl orthosilicate (TEOS, Fluka cat. no. 86578) was added quickly into the mixture, which was left to stir for 24 h. The 50 nm silica was prepared very similarly, but the volume fractions (mL) of ethanol, DI water, ammonium hydroxide, and TEOS were changed to a volume ratio of 245:3.8:8.5:7.7, respectively. After 24 h of stirring, the silica nanoparticles were placed into 12 000 MW dialysis membranes (Fisher, cat. no. 08667E) and placed into a pure ethanol bath. This bath was changed every 5 h at least four different times to remove any excess water and ammonium hydroxide not consumed in the reaction.

The 0, 6.8, 12.8, or 22.7 wt % silica particles in ethanol were added into 0.35 g of pentaerythritol triacrylate (Aldrich, cat. no. 246794). The ethanol was rotovaped from the mixture, and immediately 0.2 g of 1-vinyl-2-pyrrolidinone (NVP, Aldrich, cat. no. V3409) was added to reduce the viscosity. The photoreactive mixture was then vortexed and sonicated in a separate container in the dark. It consisted of 0.01 g of diiodofluorescein (Aldrich, cat. no. 206806), 0.1 g of NVP, 0.01 g of 30 μm glass spheres, and 0.02 g of 2,6-diisopropyl-*N*,*N*-dimethylaniline (Aldrich, cat. no. 550698). This photoreactive mixture was then added into the monomer containing the nanoparticle solution. This mixture was sandwiched between two glass slides, using 30 μm glass spacers to give the syrup a uniform thickness. The mixture was exposed by using two beams from a 532 nm frequency-doubled NdYAG laser. The angle between the two beams was approximately 30° resulting in about a 1 μm periodicity. The power density was set between 0.035 and 200 mW/cm^2 per beam. The time was varied from 6.75 to 300 s. To determine the magnitude of diffraction during the writing of the Bragg grating, a HeNe laser was placed normal to the sample and the power of the resulting first-order Bragg diffraction peak was measured and normalized to the zeroth-order peak. The zero- and first-order diffraction peaks were measured and recorded every 0.25 s. Diffraction magnitude was determined by dividing the intensity of the first-order diffraction peak by the sum of the zero- and first-order peaks. The diffraction curve of the 500 nm sample was not measured as a function of time as it was trapped by total internal reflection.

Samples were cured under a white light source for at least 20 min following the exposure. After this cure, the glass slides were broken apart and the sample was coated with approximately 20 nm of gold/palladium for ease of visibility with further imaging. The samples were then embedded into a microtome mold with Epofix epoxy and microtomed into 90 nm thick sections for viewing under a Phillips CM200 transmission electron microscope.

ACKNOWLEDGMENTS This work is supported by the National Science Foundation's Nanoscale Science and Engineering Center (NSEC) under NSF Award no. DMR-0642573, and the Air Force Research Laboratory, Materials and Manufacturing Directorate (AFRL) at Wright Patterson Air Force Base (WPAFB). Special thanks to AFRL at WPAFB for use of the facilities.

Supporting Information Available: TEM images of six different regions of the same sample to demonstrate that the micrographs are representative. This material is available free of charge via the Internet at http://pubs.acs.org.

REFERENCES AND NOTES

1. Ray, S. S.; Bousmina, M. *Polymer Nanocomposites and Their Applications*; American Scientific: Stevenson Ranch, CA, 2006.
2. Vaia, R. A.; Maguire, J. F. Polymer Nanocomposites with Prescribed Morphology: Going beyond Nanoparticle-Filled Polymers. *Chem. Mater.* **2007**, *19*, 2736–2751.
3. Chou, S. Y.; Krauss, P. R.; Renstrom, P. J. Imprint Lithography with 25-Nanometer Resolution. *Science* **1996**, *272*, 85–87.
4. Xia, Y.; Whitesides, G. M. Soft Lithography. *Annu. Rev. Mater. Sci.* **1998**, *28*, 153–184.
5. Gonsalves, K. E.; Merhari, L.; Wu, H.; Hu, Y. Organic-Inorganic Nanocomposites: Unique Resists for Nanolithography. *Adv. Mater.* **2001**, *13*, 703–714.
6. Schmidt, G.; Nakatani, A. I.; Butler, P. D.; Karim, A.; Han, C. C. Shear Orientation of Viscoelastic Polymer-Clay Solutions Probed by Flow Birefringence and SANS. *Macromolecules* **2000**, *33*, 7219–7222.
7. Martin, C. A.; Sandler, J. K. W.; Windle, A. H.; Schwarz, M.-K.; Bauhofer, W.; Schulte, K.; Shaffer, M. S. P. Electric Field-Induced Aligned Multi-Wall Carbon Nanotube Networks in Epoxy Composites. *Polymer* **2005**, *46*, 877–886.
8. Koerner, H.; Hampton, E.; Dean, D.; Turgut, Z.; Drummy, L.; Mirau, P.; Vaia, R. Generating Triaxial Reinforced Epoxy/Montmorillonite Nanocomposites with Uniaxial Magnetic Fields. *Chem. Mater.* **2005**, *17*, 1990–1996.
9. Bockstaller, M. R.; Mickiewicz, R. A.; Thomas, E. L. Block Copolymer Nanocomposites: Perspectives for Tailored Functional Materials. *Adv. Mater.* **2005**, *17*, 1331–1349.
10. Vaia, R. A.; Dennis, C. L.; Natarajan, L. V.; Tondiglia, V. P.; Tomlin, D. W.; Bunning, T. J. One-Step, Micrometer-Scale Organization of Nano- and Mesoparticles Using Holographic Photopolymerization: A Generic Technique. *Adv. Mater.* **2001**, *13*, 1570–1574.
11. Garnweitner, G.; Goldenberg, L. M.; Sakhno, O. V.; Antonietti, M.; Niederberger, M.; Stumpe, J. Large-Scale Synthesis of Organophilic Zirconia Nanoparticles and their Application in Organic-Inorganic Nanocomposites for Efficient Volume Holography. *Small* **2007**, *3*, 1626–1632.
12. Sakhno, O. V.; Goldenberg, L. M.; Stumpe, J.; Smirnova, T. N. Surface Modified ZrO_2 and TiO_2 Nanoparticles Embedded in Organic Photopolymers for Highly Effective and UV-Stable Volume Holograms. *Nanotechnology* **2007**, 105704.
13. Suzuki, N.; Tomita, Y.; Ohmori, K.; Hidaka, M.; Chikama, K. Characterization of Volume Gratings Formed in ZrO_2 Nanoparticle-Dispersed Photopolymers. CLEO/Europe and IQEC 2007 Conference Digest. 2007, p 255.
14. Sánchez, C.; Escuti, M. J.; van Heesch, C.; Bastiaansen, C. W. M.; Broer, D. J.; Loos, J.; Nussbaumer, R. TiO_2 Nanoparticle-Photopolymer Composites for Volume Holographic Recording. *Adv. Funct. Mater.* **2005**, *15*, 1623–1629.
15. Suzuki, N.; Tomita, Y.; Kojima, T. Holographic Recording in TiO_2 Nanoparticle-Dispersed Methacrylate Photopolymer Films. *Appl. Phys. Lett.* **2002**, *81*, 4121–4123.
16. Sakhno, O. V.; Smirnova, T. N.; Goldenberg, L. M.; Stumpe, J. Holographic Patterning of Luminescent Photopolymer Nanocomposites. *Mater. Sci. Eng., C* **2008**, *28*, 28–35.
17. Suzuki, N.; Tomita, Y. Silica-Nanoparticle-Dispersed Methacrylate Photopolymers with Net Diffraction Efficiency Near 100%. *Appl. Opt.* **2004**, *43*, 2125–2129.
18. Sakhno, O. V.; Goldenberg, L. M.; Stumpe, J.; Smirnova, T. N. Effective Volume Holographic Structures Based on Organic−Inorganic Photopolymer Nanocomposites. *J. Opt. A: Pure Appl. Opt.* **2009**, *11*, 024013.
19. Smirnova, T. N.; Sakhno, O. V.; Yezhov, P. V.; Kokhtych, L. M.; Goldenberg, L. M.; Stumpe, J. Amplified Spontaneous Emission in Polymer-CdSe/ZnS-Nanocrystal DFB Structures Produced by the Holographic Method. *Nanotechnology* **2009**, *20*, 245707.
20. Ostrowski, A. M.; Naydenova, I.; Toal, V. Light-Induced Redistribution of Si-MFI Zeolite Nanoparticles in Acrylamide-Based Photopolymer Holographic Gratings. *J. Opt. A: Pure Appl. Opt.* **2009**, *3*, 034004.
21. Leite, E.; Naydenova, I.; Pandey, N.; Babeva, T.; Majano, G.; Mintova, S.; Toal, V. Investigation of the Light Induced Redistribution of Zeolite Beta Nanoparticles in an Acrylamide-Based Photopolymer. *J. Opt. A: Pure Appl. Opt.* **2009**, *2*, 024016.

22. Suzuki, N.; Tomita, Y. Real-Time Phase-Shift Measurement During Formation of a Volume Holographic Grating in Nanoparticle-Dispersed Photopolymers. *Appl. Phys. Lett.* **2006**, *88*, 011105.
23. Tomita, Y.; Suzuki, N. Holographic Manipulation of Nanoparticle Distribution Morphology in Nanoparticle-Dispersed Photopolymers. *Opt. Lett.* **2005**, *30*, 839–841.
24. Goldenberg, L. M.; Sakhno, O. V.; Smirnova, T. N.; Helliwell, P.; Chechik, V.; Stumpe, J. Holographic Composites with Gold Nanoparticles: Nanoparticles Promote Polymer Segregation. *Chem. Mater.* **2008**, *20*, 4619–4627.
25. Tomita, Y.; Chikama, K.; Nohara, Y.; Suzuki, N.; Furushima, K.; Endoh, Y. Two-Dimensional Imaging of Atomic Distribution Morphology Created by Holographically Induced Mass Transfer of Monomer Molecules and Nanoparticles in a Silica-Nanoparticle-Dispersed Photopolymer Film. *Opt. Lett.* **2006**, *31*, 1402–1404.
26. Suzuki, N.; Tomita, Y. Highly Transparent ZrO_2 Nanparticle-Dispersed Acrylate Photopolymers for Volume Holographic Recording. *Opt. Express* **2006**, *14*, 12712–12719.
27. Takahashi, H.; Naito, T.; Tomita, Y. Holographic Recording in Methacrylate Photopolymer Film Codoped with Benzyl *n*-Butyl Phthalate and Silica Nanoparticles. *Jpn J. Appl. Phys.* **2006**, *45*, 5023–5026.
28. Astumian, R. D. Thermodynamics and Kinetics of a Brownian Motor. *Science* **1997**, *276*, 917–922.
29. Colvin, V. L.; Larson, R. G.; Harris, A. L.; Schilling, M. L. Quantitative Model of Volume Hologram Formation in Photopolymers. *J. Appl. Phys.* **1997**, *81*, 5913–5923.
30. Zhao, G.; Mouroulis, P. Diffusion Model of Hologram Formation in Dry Photopolymer Materials. *J. Mod. Opt.* **1994**, *41*, 1929–1939.